

Dirk Ziegenbalg¹
Benjamin Wriedt¹
Günter Kreisel²
Dana Kralisch³

Investigation of Photon Fluxes within Microstructured Photoreactors Revealing Great Optimization Potentials

¹Institut für Technische Chemie,
Universität Stuttgart, Stuttgart,
Germany.

²Institut für Technische Chemie
und Umweltchemie, Friedrich-
Schiller-Universität Jena, Jena,
Germany.

³Institut für Pharmazie, LS für
Pharmazeutische Technologie,
Friedrich-Schiller-Universität
Jena, Jena, Germany.

A simple model for determining potential bottlenecks of a photoreactor setup focusing on the photon fluxes is presented. The application of the concept can reveal optimization potentials and gives insights into the sensitivity of the reactor setup to different optimization possibilities. The introduced model benefits from the concept of using only data already available from optimization studies of the process conditions. Applying the introduced concept to the characterization of a previously developed modular organic light-emitting diode reactor setup revealed great optimization potentials, especially with respect to the external photonic efficiency. Interestingly, the attempt to enhance the external photonic efficiency by increasing the projection area of the reactor did not provide any improvement. This is attributed to a significant influence of reflection and scattering within the setup.

Keywords: Microstructured photoreactor, Organic light-emitting diode, Photochemistry, Photon flux

Received: August 22, 2015; *revised:* November 03, 2015; *accepted:* November 09, 2015

DOI: 10.1002/ceat.201500498



Supporting Information
available online

1 Introduction

Flow or microstructured photoreactors have found widespread application in the field of synthetic organic chemistry during the last years [1–4]. The small dimensions of these reactors accelerate the mass and heat transfer. Therefore, even very demanding reactions such as direct fluorinations or ethoxylations can be conducted safely [5–7]. An additional benefit of this kind of reactor is the enhanced reaction control, which results from the acceleration of transport processes [8]. Thereby, the acceleration is due to the reduction of characteristic time scales owing to the typically small overall dimensions. Furthermore, continuous processes can easily be investigated in lab scale. The small channel heights ensure a high photon flux within the whole reaction volume and a minimum of non-irradiated volumes [9]. Small internal volumes further ensure safe processing even of highly explosive systems such as methanol/oxygen [10, 11]. Recent work aims at improving flow photoreactors in terms of practical flexibility which is realized by the use of capillaries instead of dedicated flow reactors and also by an increase of the inner diameter of the channels [12–16]. This enables among others the use of higher flow rates while ensuring the same irradiation time or accounting for physical constraints such as solubility limits, maintaining a sufficient light absorption.

Despite the increasing number of applications of microstructured photoreactors, publications on reactor characteristics

and/or the interplay between the light source and the reactor geometry are rare. Pioneering work on this topic was published by the group of Loubiere with work on accurate comparison of batch and microstructured photoreactors in terms of an engineering analysis [17]. The results demonstrate that the often emphasized superior performance of flow reactors can be partly explained by an incorrect comparison of criteria such as conversion, productivity or space-time yield. Ensuring comparable conditions by realizing the same power received and photonic efficiency results in a similar performance. From the practical side, such a comparison requires the estimation of the photon flux within the reaction channel. For macroscopic photoreactors the photon flux can be determined either by physical detectors or chemical actinometry [18].

For micro- or mesoscopic reactors the option of physical detectors must be excluded since the available detectors do not fit into the reaction channel. Even if such detectors were available in a suitable size, care should be taken since the installation of a detector within a channel disturbs the fluid dynamics and with this possibly the actual photon flux. The latter point becomes relevant when photochemical systems are used which produce an inner filter by the reaction itself [19]. With this, chemical actinometry is the method of choice if micro- or mesostructured photoreactors shall be characterized [20]. Nevertheless, the drawbacks of this method are the following: i) additional experiments have to be performed to determine the photon flux in the photoreactor; ii) the photoreactor cannot be characterized under real reaction conditions since the actual reaction is not taking place; iii) actinometry is usually sensitive to a broad range of wavelengths and with this, the photon flux is always the integral of all emitted wavelengths.

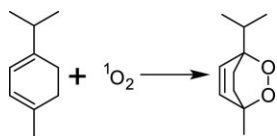
Correspondence: Dr. Dirk Ziegenbalg (dirk.ziegenbalg@itc.uni-stuttgart.de), Institut für Technische Chemie, Universität Stuttgart, Pfaffenwaldring 55, 70569 Stuttgart, Germany.

The sensitivity for several wavelengths can be considered by subsequent mathematical considerations, but in the narrow sense, it can only be done easily if effects such as reflection or scattering, which are wavelength-dependent, can be excluded. Especially for micro- and mesostructured photoreactors, these assumptions are not always allowed since the cross section of the channels is often not a rectangle but a circle and with this the angle of incidence significantly differs from 90°. Further fabrication methods such as sandblasting of glass lead to rough surfaces causing an increased influence of scattering.

Considering all the points above it becomes clear that characterizing photoreactors is accompanied by a considerable effort in addition to the work of optimizing process conditions for the actual conditions. Hence, a general approach for characterizing micro- and mesostructured photoreactors starting from available data obtained during process optimization will be presented within this article. It will be shown which insights into the efficiency of the reactor setup can be gained just by simply closing the photon balance [21].

2 Experimental

The synthesis of ascaridole from α -terpinene and $^1\text{O}_2$ as indicated in Scheme 1 was used as a test reaction [22].



Scheme 1. Reaction scheme of the ascaridole synthesis.

The corresponding experimental setup is presented in Fig. 1. The general flow chart is depicted in Fig. S1 of the Supporting Information. A detailed description of the reactor modules can be found in [23]. For the experiments, a varying number of modules and organic light-emitting diodes (OLEDs; OSRAM CDW-031) were used, depending on the actual requirements of the investigated parameter. Except where otherwise stated, the setup was comprised of three modules equipped with one OLED per module. In general, the reactors were made of borosilicate glass with round channels of 1 mm inner diameter and 1.6 m channel length per module (Little Things Factory GmbH, Ilmenau, Germany). Each reactor had an internal volume of 1.256 mL. The reactants were pumped with syringe pumps (neMESYS, cetoni GmbH, Korbußen, Germany). For each fluid two syringe pumps were coupled to realize continuous fluid delivery. The fluids were merged in a T-junction. Depending on the process conditions, a stable slug flow or an annular flow resulted. The feeding and connecting tubes were shielded from ambient light by aluminum foils.

Methanol served as solvent. All compounds were used as received without further purification. The typical starting concentration of α -terpinene was $c_{\text{Terp}}^{1)} \approx 0.14 \text{ mol L}^{-1}$. The purity of α -terpinene was declared to be $\geq 85\%$ but varied depending

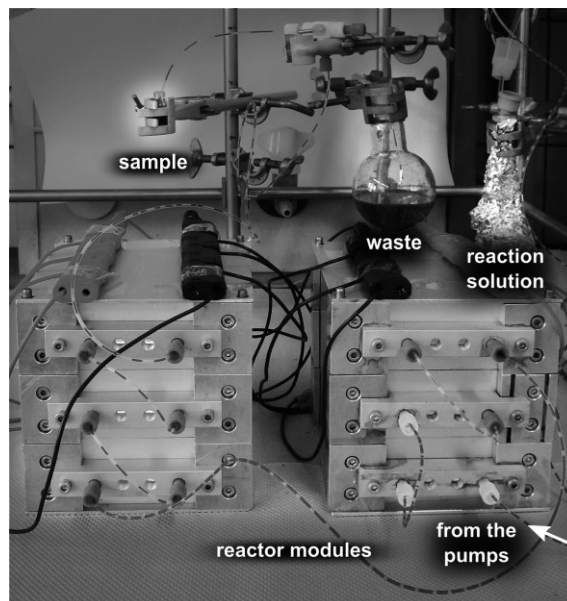


Figure 1. Setup with two stacks with three modules each. Aluminum foils shielding the tubes from light were removed for clarification.

on the production lot. Therefore, the purity of the reaction solution was determined by GC measurements before reaction and the actual concentration was used for further calculations. Pure oxygen was employed to provide $^3\text{O}_2$ to the liquid phase. As sensitizer rose bengal was used with a concentration of $c_{\text{RB}} = 0.0049 \text{ mol L}^{-1}$. This high concentration allowed the absorption of almost all photons reaching the reaction solution within the specific wavelength range. The absorbance of the reaction solution in a 1-mm cuvette is displayed in Fig. 2 a. For comparison, the absorption spectrum of rose bengal is given in Fig. 2 b. Because of the small amount of substances which were collected, the conversion of the α -terpinene was monitored by GC measurements on a Varian CP-3900 apparatus equipped with a HP-5 column (30 m, $0.25 \mu\text{m}$, $d = 0.32 \text{ mm}$, $3 \text{ mL min}^{-1} \text{ N}_2$; FID detector; injector temperature 175°C , split injection mode, $1 \mu\text{L}$; 35°C maintained for 1 min, then ramped to 240°C at 20 K min^{-1}). *n*-Dodecane was taken as internal standard. The spectral irradiance of the OLEDs was measured by Carl Zeiss AG (Jena, Germany) with a CAS140CT-154 spectrometer (Instrument System, Munich, Germany) using an ISP250 integrating sphere (Instrument System). A photon flux of $q_{n,p,\text{OLED}} = 2.0 \times 10^{-7} \text{ Es}^{-1}$ ($\pm 10\%$) for the whole spectral domain was calculated for one CDW-031 OLED panel from a radiant power of $P_{e,\text{OLED}} = 41.4 \text{ mW}$ (Fig. 2). The emission area of the OLEDs was $S_{\text{OLED}} = 4.9 \times 10^{-3} \text{ m}^2$.

For residence time measurements, two UV/VIS flow-through cells were installed in front and behind the reactor. With this, it was possible to measure both the entrance and the exit signal and, therefore, minimize the influence of the periphery. The setup is schematically illustrated in Fig. S8. The residence time distribution was measured via an impulse response experiment. To ensure minimum differences to the actual reactions, the same composition of the reaction solution was used except the

1) List of symbols at the end of the paper.

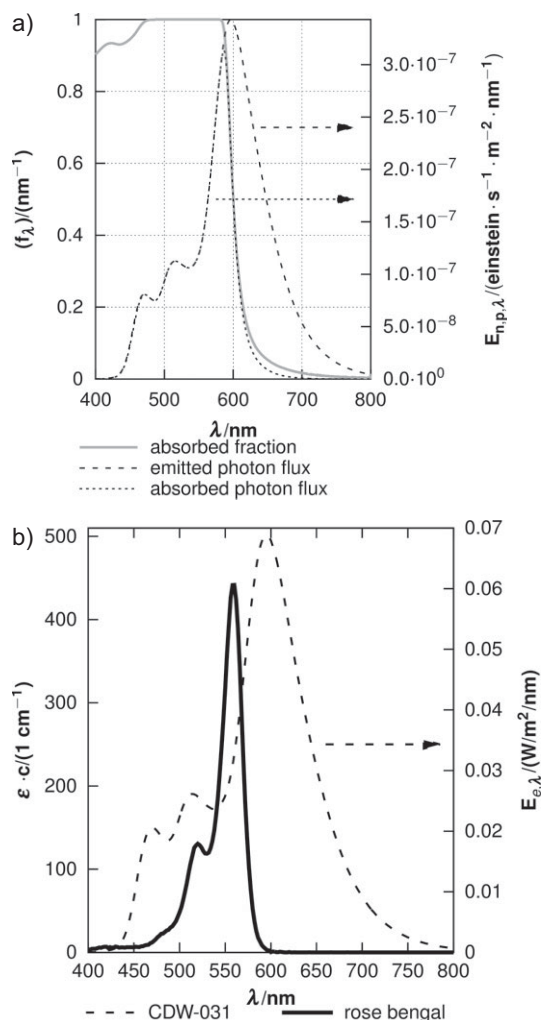


Figure 2. Absorption spectrum of the investigated rose bengal solutions. (a) Spectral absorption fraction f_λ with $c_{\text{RB}} = 0.0049 \text{ mol L}^{-1}$ and 1 mm optical path and emitted photon irradiance of CDW-031 OLEDs; (b) emission and absorption spectrum of CDW-031 OLEDs and rose bengal, respectively.

sensitizer. A small amount of rose bengal was injected as a tracer with a six-port valve at $t = 0$.

The general process conditions were initially chosen in such a manner that the complete range of conversions could be covered. To achieve this, the total flow rate \dot{V} of the two fluids and the stoichiometric input ratio of oxygen to reactant $r_{\text{O}_2/\text{RL}}$ were varied in all studies. The stoichiometric input ratio is defined as the amount of oxygen entering the reactor per time divided by the amount of organic reactant entering the reactor per time:

$$r_{\text{O}_2/\text{terp}} = \frac{\dot{n}_{\text{O}_2}}{\dot{n}_{\text{terp}}} \quad (1)$$

The flow rate mainly influences the residence time while the stoichiometric input ratio affects the flow conditions, i.e., stable slug flow or annular flow, and the liquid's projection area; see [23] for an illustration. Using $r_{\text{O}_2/\text{terp}} = 0.5$, a stable slug flow

could be observed. Increasing $r_{\text{O}_2/\text{terp}}$ led to a transition to an annular flow. More details on the flow conditions are given in a previous publication [23].

The measured conversions were fitted by utilizing an ANOVA with the program Design Expert (Stat Ease Inc.) to derive deeper insights on the interactions. Especially the annular flow conditions led to difficulties in reproducibility, since the liquid flow rate at the exit was not constant. These difficulties were counteracted by repeated measurements and statistical data handling. Measurements were repeated at least two times. Outliers were removed when statistically suggested by the program. In most cases, the conversion was transformed into a logit representation for the ANOVA ensuring that the fitting surfaces gave only values between 0 and 100 %. The resulting equations were then used for the graphical representations.

As parameters for the fits, the total flow rate \dot{V} and the stoichiometric input ratio $r_{\text{O}_2/\text{terp}}$ were used. With this, the obtained fits do not have a direct meaning in terms of fundamental units such as reaction time or concentration. Hence, the fitting parameters were not employed for quantitative comparisons but for the identification of trends and dependencies. The results of the ANOVA are represented as hypersurfaces in the diagrams. The black circles denote experimental values lying above the determined hypersurface and gray squares indicate experimental values lying below the hypersurface. This representation was chosen to help reading the 3D plots.

3 Results and Discussion

3.1 Mass Transfer

Before acquiring a deeper knowledge about the efficiency of the used reactor system, a series of initial experiments had to be conducted. The mass transfer or photon flux usually limit photooxygenations [24]. Hence, both parameters were investigated to determine the limiting parameter for the investigated reactor system.

Gas/liquid mass transfer might limit two-phase reactions due to the fact that the involved fluids are not mixable. Investigations on the influence of the g L^{-1} mass transfer were conducted by variation of the oxygen partial pressure in the gas phase. This was realized by the installation of a backpressure valve and the use of air instead of pure oxygen. With the backpressure valve and pure oxygen, an overpressure of 1.36 bar was realized. Assuming that Henry's law is valid, these measures increase the equilibrium concentration of oxygen from $c_{\text{O}_2} \approx 0.0021 \text{ M}$ to $\approx 0.0103 \text{ M}$ and $\approx 0.0243 \text{ M}$, respectively [25].

The results reveal that within the accuracy of the measurements, the oxygen concentration has no significant influence on the overall reaction rate and with that, the oxygen mass transfer is not limiting the reaction rate (see Fig. S2).

3.2 Photon Flux

To investigate the influence of the photon flux, the reactor set-up was adapted in such a manner that the number of glass reactors was kept constant, while the number of OLEDs was varied. Therefore, three modules were used and equipped with one, two, three or six OLEDs. The configurations are displayed in Fig. S3. The use of an unaltered number of glass reactors ensured that the residence times and the flow conditions were constant for all experiments.

The results reveal a positive dependence of the converted concentration on the number of OLEDs. Fig. 3 depicts the findings exemplarily; see also Fig. S4. These experiments prove that the overall reaction rate is limited by the photon flux, which would correspond to a pseudo zero-order reaction rate with respect to α -terpinene and therewith a linear dependency. A strictly linear increase of the conversion with the number of OLEDs was expected due to the similar performance of each OLED. Indeed, a linear dependency was found for flow rates of $\dot{V} = 3.25$ and 6 mL min^{-1} . For low flow rates where full conversion is reached, the actual dependency cannot be resolved. Deviations from a slope of 1 result from the influence of absorption, scattering, and reflection at all parts within the reactor module. The hypersurface drawn in Fig. 3 cannot perfectly map the experimental results due to the limited polynomial description which was available in the utilized software.

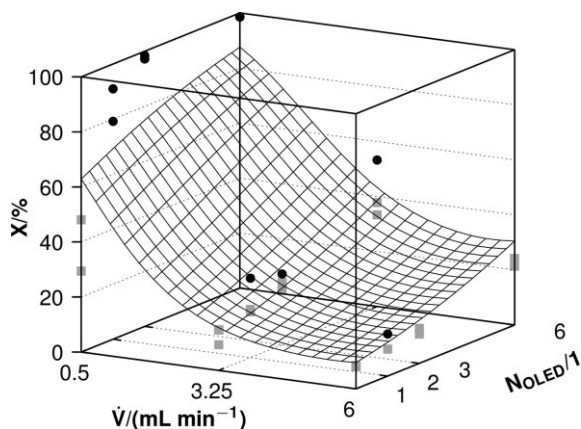


Figure 3. Conversion of α -terpinene as a function of the number of OLEDs and \dot{V} at $r_{O_2/terp} = 10.25$.

Reflection within a reactor stack housed by aluminum parts can have a significant influence on the photon flux utilizable within the microchannels. To investigate the influence of reflection, a reactor setup with three modules was lined with black fleece to minimize reflection. The resulting setup is shown in Fig. S5.

The results for experiments with and without minimized reflection are depicted in Fig. 4. A comparison revealed that the complete hypersurface is shifted to lower values by a constant difference of 6.5 % when reflection is diminished. For process conditions with a low conversion this implies that a significant amount of up to 60 % of the utilized photon flux can be ascribed to reflection. This result is important when the efficiency of the whole reactor setup shall be determined.

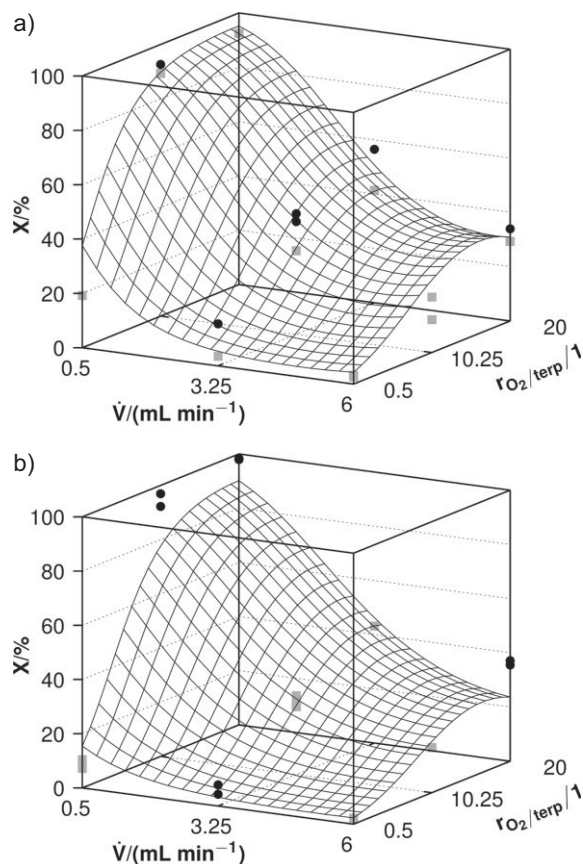


Figure 4. Conversion of α -terpinene as a function of \dot{V} and $r_{O_2/RL}$; (a) with reflection; (b) without reflection.

3.3 Residence Time

In order to completely characterize the reactor system, the actual residence times for different process conditions were measured. The results are presented in Fig. S9. The figures demonstrate that the actual residence time τ is significantly different to the space time t_R proving that the assumption of plug flow characteristics for the obtained flow conditions is not entirely valid. The deviations can raise up to a factor of 4 for high $r_{O_2/terp}$. For further results see the Supporting Information.

The results of the residence time determination are of general importance when kinetic information shall be extracted from experimental data. Due to the significant deviations between experimental and theoretical residence time, it is crucial to determine the actual residence time for such gas-liquid systems.

These initial investigations reveal that the photon flux is indeed the limiting factor under the investigated process conditions. Besides, it was found that reflection significantly influences the conversion and must, therefore, be included into estimations as well as the actual residence time.

3.4 Energetic Efficiency

3.4.1 Theoretical Considerations

To optimize a photochemical reactor setup and with this the potential of the setup in terms of, e.g., productivity, space-time yield or similar key figures, it is crucial to understand the interplay between the light source(s) and the reactor.

With regard to the investigated reaction, an optimization basically requires an increase of the incident photon flux within the reaction channels. To achieve this, potential bottlenecks should be identified by establishing a photon balance. Such a balancing initially leads to the general radiative transfer equation [21]:

$$\left| \begin{array}{c} \text{time rate of} \\ \text{change of} \\ \text{photon flux} \end{array} \right| + \left| \begin{array}{c} \text{net photon flux} \\ \text{leaving the system} \\ \text{across surface A} \end{array} \right| = \left| \begin{array}{c} \text{net gain of photons} \\ \text{owing to emission,} \\ \text{absorption, in-} \\ \text{and out - scattering} \\ \text{in volume V} \end{array} \right| \quad (2)$$

The time rate of change of photon flux can be neglected for the investigated system since the emitted photon flux of the light sources utilized was constant. With respect to the right side of Eq. (2), emission and in- and out-scattering do not play an important role for the investigated photooxygenation in a homogeneous solution. Thus, absorption is the only process that has to be considered. By approximating the reactor geometry as a rectangular domain and the light source as an unidirectional emitter, similar to the approach of Aillet et al. [19], the general balance can be transformed to:

$$\frac{dE_{n,p,\lambda}}{ds} = -\alpha(\lambda)E_{n,p,\lambda} \quad (3)$$

with $E_{n,p,\lambda}$ being the spectral photon irradiance in $\text{E m}^{-2}\text{s}^{-1}\text{nm}^{-1}$ within the reaction channel and $\alpha(\lambda)$ being the volumetric napierian absorption coefficient in m^{-1} . $\alpha(\lambda)$ can be calculated from the Lambert-Beer law as long as the constraints, most important a sufficiently high dilution, are fulfilled by:

$$\alpha(\lambda) = \varepsilon(\lambda)c \quad (4)$$

with $\varepsilon(\lambda)$ being the napierian molar absorption coefficient in $\text{m}^2\text{mol}^{-1}$ and c being the amount concentration in mol m^{-3} .

Due to the polychromatic emission of the OLEDs, the spectral photon irradiance and the napierian molar absorption coefficient, Eq. (3) has to be integrated over all emitted wavelengths from λ_0 to λ_1 :

$$\int_{\lambda_0}^{\lambda_1} \frac{dE_{n,p,\lambda}}{ds} = \int_{\lambda_0}^{\lambda_1} -\alpha(\lambda)E_{n,p,\lambda} \quad (5)$$

The spectral photon irradiance $E_{n,p,\lambda}$ is determined primarily by the performance of the light source and the efficiency of irradiating the reactor. While the first aspect is given by the

light source itself, the latter aspect originates from the geometry of the reactor and the overall setup. The efficiency of the light source, which could not be optimized during the course of the investigations, is given by the luminescent efficiency η_{lum} :

$$\eta_{\text{lum}} = \frac{P_{\text{OLED},e}}{P_{\text{el}}} \quad (6)$$

where $P_{\text{OLED},e}$ is the radiant power of the OLED and P_{el} is the used electrical power.

The most simple approximation of $E_{n,p,\lambda}$ can be done by assuming that all emitted photons are directed rectangular to the reactor and that photons only initiate a reaction within the actual reaction channel neglecting all optical processes but absorption.

Consequently, the irradiated projection area of the reactor S_R has to be compared with the effective emission area of the light source S_{OLED} . From these assumptions, the maximal photon flux $q_{n,p,R}$, which can be absorbed, is given by:

$$q_{n,p,\lambda,R} = E_{n,p,\lambda}S_R \quad (7)$$

$$q_{n,p,R} = \int_{\lambda_0}^{\lambda_1} E_{n,p,\lambda}S_R = E_{n,p}S_R \quad (8)$$

The efficiency η_S of the setup can thus be determined by comparison with the emitted photon flux $q_{n,p,\text{OLED}}$:

$$q_{n,p,\text{OLED}} = E_{n,p,\text{OLED}}S_R \quad (9)$$

$$\eta_S = \frac{q_{n,p,R}}{q_{n,p,\text{OLED}}} = \frac{E_{n,p}S_R}{E_{n,p,\text{OLED}}S_{\text{OLED}}} = \frac{S_R}{S_{\text{OLED}}} \quad (10)$$

The dependency of light absorption on the optical path length as well as the wavelength dependency of the absorption coefficient require additional considerations. For diluted solutions, this can be done by using the Lambert-Beer law. For solutions with high concentrations, which are typically used for microstructured photoreactors, the actual volumetric napierian absorption coefficient $\alpha(\lambda)$ has to be determined experimentally.

After variable separation and integration over the optical length s , the spectral photon irradiance Eq. (5) transforms to:

$$\int_{\lambda_0}^{\lambda_1} \ln \frac{E_{n,p,\lambda,1}}{E_{n,p,\lambda,0}} = \int_{\lambda_0}^{\lambda_1} \alpha(\lambda)s \quad (11)$$

$$\int_{\lambda_0}^{\lambda_1} -A(\lambda) = s \int_{\lambda_0}^{\lambda_1} \alpha(\lambda) \quad (12)$$

which is basically the Lambert-Beer law accounting for nonideal conditions when experimental absorbance values A are

used. The fraction of photons absorbed, given by the absorption factor f , can thus be calculated by:

$$f = \int_{\lambda_0}^{\lambda_1} 1 - \frac{E_{n,p,\lambda,1}}{E_{n,p,\lambda,0}} = \int_{\lambda_0}^{\lambda_1} 1 - \exp(-A(\lambda)) = \eta_{\text{abs}} \quad (13)$$

From a contextual view, the absorption factor f represents the efficiency of absorbing photons η_{abs} . A scaling to the emission and absorption areas is not required since the degree of absorption only depends on the optical length, which is equal to the channel height and, therefore, constant for the investigated reactor system. It is important to note that the above equation is only valid as long as the optical path length in the reactor and for the absorbance measurements are equal.

As a last parameter influencing the amount of photons which initiate a reaction, the quantum yield of singlet oxygen generation ϕ should be considered. This assumption is only valid for very reactive systems as the ascaridole synthesis, where almost all generated $^1\text{O}_2$ is consumed instantaneously [26]. In this case, losses due to deactivation of $^1\text{O}_2$ can be neglected. The quantum yield ϕ , which is equal to an efficiency, can usually be taken from the literature [26, 27].

With the above considerations on relevant processes, the photon flux q_{inc} actually initiating a reaction can be calculated as follows:

$$q_{\text{inc}} = N_{\text{OLED}} q_{n,p,\text{OLED}} \eta_S \eta_{\text{Abs}} \phi \quad (14)$$

$$q_{\text{inc}} = N_{\text{OLED}} (E_{n,p,0} S_{\text{OLED}}) \left(\frac{S_R}{S_{\text{OLED}}} \right) \left(\int_{\lambda_0}^{\lambda_1} 1 - \exp(A(\lambda)) \right) \phi \quad (15)$$

$$q_{\text{inc}} = N_{\text{OLED}} E_{n,p,0} S_R \left(\int_{\lambda_0}^{\lambda_1} 1 - \exp(A(\lambda)) \right) \phi \quad (16)$$

with N_{OLED} being the number of OLEDs used for the experiment. The photon flux q_{inc} represents a theoretical maximum when processes like reflection or scattering are neglected and only absorption within the reaction solution is relevant. For a given system, q_{inc} can be compared to the macroscopic (overall) rate of conversion $\dot{\xi}$ which is observed for certain reaction conditions yielding the photonic efficiency ξ [28]:

$$\xi = \frac{\dot{\xi}}{q_{\text{inc}}} = \frac{c_{\text{terp},0} X \dot{V}_1}{q_{\text{inc}}} \quad (17)$$

For the characterization of the light-source-reactor-setup an extension of the definition of ξ seems suitable in such a way that the macroscopic reaction rate \dot{n} is compared to the emitted photon flux $q_{n,p,\lambda,\text{OLED}}$. By doing this, a quantity is obtained which represents an external photonic efficiency ξ_{ext} quantifying the actual photon utilization of the whole setup:

$$\xi_{\text{ext}} = \frac{\dot{\xi}}{q_{n,p,\text{OLED}}} \quad (18)$$

Such a comparison gives an insight into the efficiency of the irradiation. Furthermore, the degree of photon utilization η_{Σ} can be calculated from q_{inc} and $q_{n,p,\text{OLED}}$, which is constant for each investigated setup:

$$\eta_{\Sigma} = \frac{q_{\text{inc}}}{q_{n,p,\text{OLED}}} = \eta_S \eta_{\text{Abs}} \phi \quad (19)$$

For the system under investigation in this work it was previously shown that a conversion of $X_{\text{refl},3} = 6.5\%$ can be attributed to reflection if three modules/OLEDs are used. Assuming that reflection is equal in every module, a conversion of $X_{\text{refl},1} = 2.16\%$ per OLED is caused by reflection. Taking the number of OLEDs for each experiment into account, the rate of conversion $\dot{\xi}_{\text{refl}}$ attributed to reflection can be calculated:

$$\dot{\xi}_{\text{refl}} = \dot{n}_{\text{refl}} = \dot{V}_1 c_0 X_{\text{refl},1} N_{\text{OLEDs}} \quad (20)$$

where \dot{V}_1 is the flow rate of the liquid phase and c_0 is the initial concentration of the reactant. With this, Eq. (16) transforms to:

$$\begin{aligned} q_{\text{inc,refl}} &= N_{\text{OLED}} E_{n,p,0} S_R \left(\int_{\lambda_0}^{\lambda_1} 1 - \exp(A(\lambda)) \right) \phi + \dot{\xi}_{\text{refl}} \\ &= N_{\text{OLED}} \left(E_{n,p,0} S_R \left(\int_{\lambda_0}^{\lambda_1} 1 - \exp(A(\lambda)) \right) \phi + \dot{V}_1 c_0 X_{\text{refl},1} \right) \end{aligned} \quad (21)$$

Thus, η_{Σ} cannot simply be calculated by using the efficiencies but by the actual photon flux $q_{\text{inc,refl}}$:

$$\eta_{\Sigma,\text{refl}} = \frac{q_{\text{inc,refl}}}{q_{n,p,\text{OLED}}} \quad (22)$$

Tab. 1 compiles the derived quantities used to characterize the photoreactor setup and to determine the photon flux.

3.4.2 Characterization of the Utilized Reactor System

The developed concept of characterizing the photoreactor system was applied to the modular OLED reactor system. The relevant constant numbers as well as the resulting efficiencies are summarized in Tab. 2.

The luminescent efficiency has been previously reported to be $\eta_{\text{lum}} = 6.4\%$ [23]. η_S can be calculated from the respective areas to be 36.8% . The areas are illustrated in a scaled manner in Fig. 5.

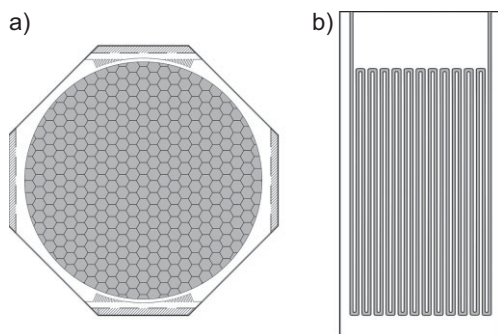
To account for the high concentration of the sensitizer, the absorbance was not calculated but measured with a 1-mm cuvette by a Varian Cary 5000 UV-VIS-NIR spectrometer (see Fig. 2 a). Below around 575 nm almost all photons are absorbed, while photons with a longer wavelength are absorbed

Table 1. Definition and description of efficiencies used to characterize the reactor setup.

Quantity	Mathematical definition	Description
η_S	$\frac{S_R}{S_{\text{OLED}}}$	Overlap of emission and reactor area
$\eta_{\text{abs}} = f$	$\int_{\lambda_0}^{\lambda_1} 1 - \exp(-A(\lambda))$	Absorbed fraction of photons with respect to polychromatic emission
ξ_{ext}	$\frac{\xi}{q_{n,p,\text{OLED}}}$	Efficiency of the overall setup consisting of light source, reactor, and all periphery
η_{Σ}	$\frac{q_{\text{inc}}}{q_{n,p,\text{OLED}}}$	Overall efficiency of the reactor system
$\eta_{\Sigma, \text{ refl}}$	$\frac{q_{\text{inc, refl}}}{q_{n,p,\text{OLED}}}$	Overall efficiency of the reactor system corrected for reflection

Table 2. Relevant numbers used to characterize the OLED reactor setup with CDW-031 OLEDs.

S_R [m ²]	S_{OLED} [m ²]	η_{lum} [%]	η_S [%]	η_{abs} [%]	ϕ [%] [27]	$\eta_{\Sigma, \text{ refl}}$ [%]
1.8×10^{-3}	4.9×10^{-3}	6.43	36.8	55.1	80	16.2

**Figure 5.** Comparison of (a) the emission area of the OLEDs and (b) the projection area of the reaction modules. The relevant areas are marked in gray and the figures are drawn in a scaled manner.

only partially. Due to the high sensitizer concentration, $\eta_{\text{abs}} \approx 55.1\%$ is observed.

It becomes clear that more than 60 % of the emitted photons are lost due to a poor overlap of emission area of the light source and projection area of the reactor. Furthermore, a significant fraction of emitted photons is lost because of the mismatch of the emission and absorption spectra. Taking the quantum yield of singlet oxygen generation ϕ into account, a process conditions-independent maximum degree of photon utilization for the investigated reactor system of $\eta_{\Sigma, \text{ refl}} \approx 16\%$ (not considering η_{lum}) can be found. This translates into a loss of photons of over 80 %, highlighting the importance of an optimized design of microstructured photoreactors. Fig. 6 illustrates the losses graphically.

The photonic efficiency ξ as a function of the process conditions is depicted in Fig. 7; for other $r_{\text{O}_2/\text{terp}}$ see Fig. S10. The calculations show that ξ depends slightly on the number of modules indicating that the simple linear correlation chosen to describe the reflection is not fully explaining the reflection influence. An increase of the number of modules decreases the photonic efficiency ξ . This points out that the influence of other optical processes such as absorption and scattering at parts other than the reactor increases with the number of modules. Furthermore, the results reveal that the photonic efficiency increases with increasing flow rate \dot{V} . This dependency results from the used g-L flow.

Assuming an ideal slug flow without liquid film on the channel walls would lead to a reduction of the projection area, since the reaction can only take place in the liquid slugs. Within the gas bubbles, photons are not absorbed and consequently the efficiency decreases. Ideal conditions as described are hardly never observed during the course of investigation. Typically, a liquid film remains on the channel walls. The film thickness increases with higher flow rate, resulting in an expansion of the effective projection area of the liquid and with this in an increase of the actual efficiency [29]. The same effect explains the enhancement of the actual efficiency with decreasing input ratio $r_{\text{O}_2/\text{terp}}$. The liquid fraction increases with decreasing ratio and the projection area becomes larger. In general, using a high input ratio $r_{\text{O}_2/\text{terp}}$ reduces the efficiency.

The dependency of the external photonic efficiency ξ_{ext} on the process parameters is displayed in Fig. 8; for results with three modules see Fig. S11. Similar to the photonic efficiency the external photonic efficiency depends on the number of modules. In addition, the influence of the flow rate depends on the stoichiometric input ratio. With $r_{\text{O}_2/\text{terp}} = 0.5$, the external photonic efficiency increases with decreasing flow rate. With $r_{\text{O}_2/\text{terp}} = 10.25$, almost no influence of the flow rate is observed, whereas with $r_{\text{O}_2/\text{terp}} = 20$ the external photonic efficiency increases with higher flow rate. These dependencies differ from those of the photonic efficiency. The difference is reasoned by the correction for reflection of ξ .

Since the number of OLEDs per reaction module could be varied, it was investigated whether this parameter has an influ-

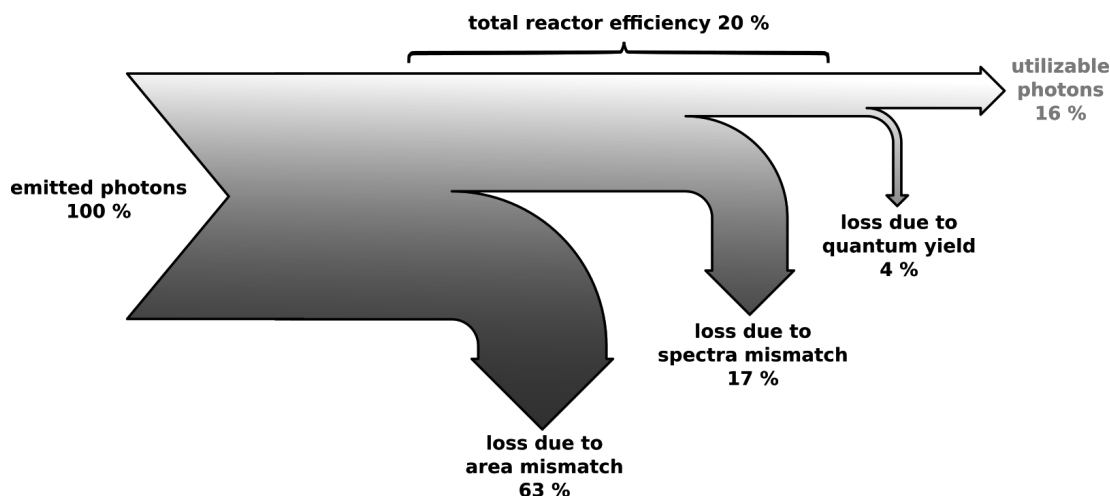


Figure 6. Photon losses within the investigated reactor system.

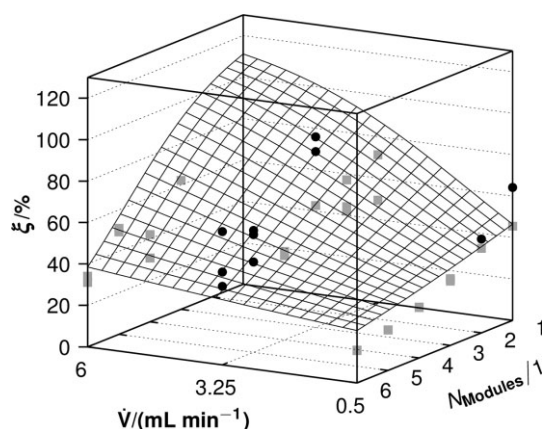


Figure 7. Photonic efficiency ξ as a function of the number of modules and \dot{V} at $r_{\text{O}_2/\text{terp}} = 10.25$.

ence on the external photonic efficiency ξ_{ext} . An analysis of the data revealed that in general the use of one OLED per module results in a significantly higher efficiency than the use of two OLEDs. Fig. 9 illustrates these findings for a setup with three modules taking $r_{\text{O}_2/\text{terp}} = 10.25$ as an example. One reason for the reduced efficiency is the way the OLEDs are installed in the modules. In case that one OLED per module is installed, the light which is not absorbed can be reflected by the back of the OLED installed in the lower module. When two OLEDs are used, the light that is not absorbed is not reflected since the second OLED is installed on the other side of the glass reactor. Hence, the influence of reflection is decreased and with this the external photonic efficiency. This finding also indicates that the before-assumed linear correlation for the reflection correction in Eq. (21) is only allowed for setups with one OLED per module.

3.5 Productivity

The productivity which is equal to the rate of conversion for a pseudo zero-order reaction, defined as:

$$\dot{\xi} = \frac{\Delta n_{\text{Terp}}}{t} = X c_{\text{Terp},0} \dot{V}_1 \quad (23)$$

is one performance criteria which is relevant when an industrial application is considered. Fig. 10 shows the dependency of the productivity on the process conditions when utilizing one OLED per module. It becomes clear that the productivity can be significantly enhanced when $r_{\text{O}_2/\text{terp}} = 0.5$ is used. This is attributed to the higher fraction of reaction solution which is pumped through the reactor when a low ratio $r_{\text{O}_2/\text{terp}}$ is applied, leading to an increased amount of reactant per time. While these results are promising, the productivity should not be assessed as a sole parameter. For example, the conversions measured for the process conditions with the largest productivity are below 10 %. Choosing such process conditions would lead to a high effort for downstream processing.

Taking the previous results into account, it could be suggested to use an increased number of reaction modules, sufficient to reach maximum conversion, a minimum input ratio, and a high flow rate. These conclusions also hold for the use of two OLEDs per module (see Fig. S12). A comparison of the productivity of the investigated reaction system with systems published in literature has been reported previously [23].

3.6 Adapted Reactor Modules

Based on the above-described results, the reactor system was improved. First, second-generation OLEDs (CDW-030) were used for further investigations. This measure was intended to account for the identified limitation of the reaction by the photon flux. A photon flux of $q_{n,p,\text{OLED}} = 3.7 \times 10^{-7} \text{ mol s}^{-1} (\pm 10 \%)$ was calculated for one CDW-030 OLED panel. Second, reactor modules were adapted in such a manner that two glass reactors

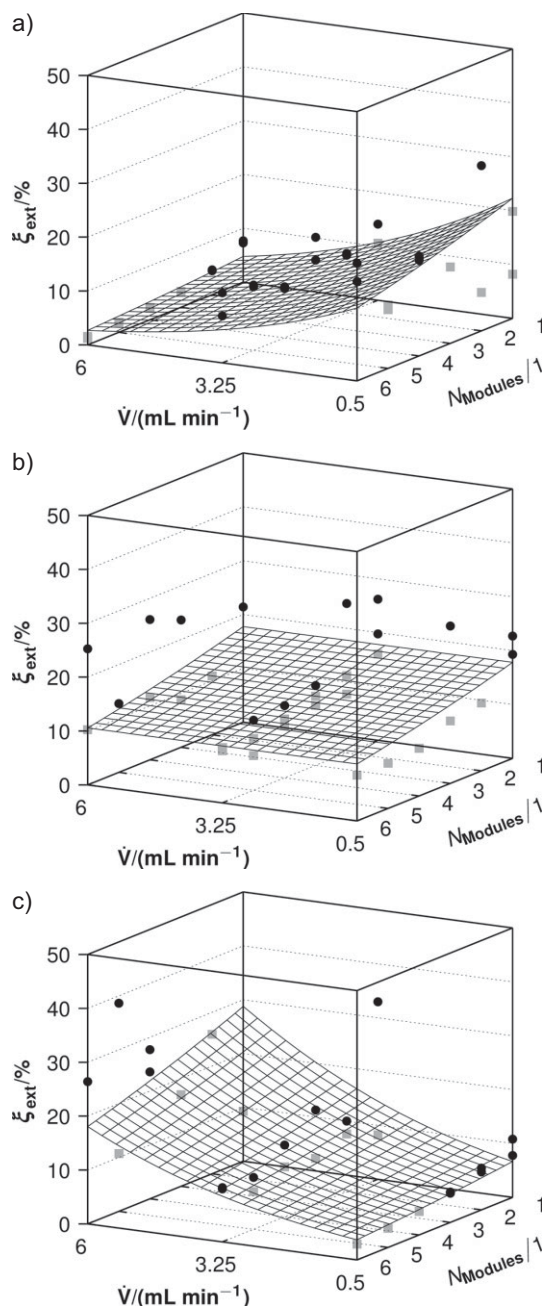


Figure 8. External photonic efficiency ξ_{ext} as a function of the number of modules and \dot{V} at (a) $r_{\text{O}_2/\text{terp}} = 0.5$, (b) $r_{\text{O}_2/\text{terp}} = 10.25$, and (c) $r_{\text{O}_2/\text{terp}} = 20$ when utilizing one OLED per module.

could be installed in one module. This module was manufactured in two versions, one, where the glass reactors were horizontally aligned and one, where the reactors were shifted against each other by 1 mm, being equal to the space between two parallel sections of the reaction channel in the glass reactors.

Fig. 11 illustrates the differences between the setups with two reactors. A comparison of the actual reactors is given in Fig. S13. Assuming that the previously made assumption of the

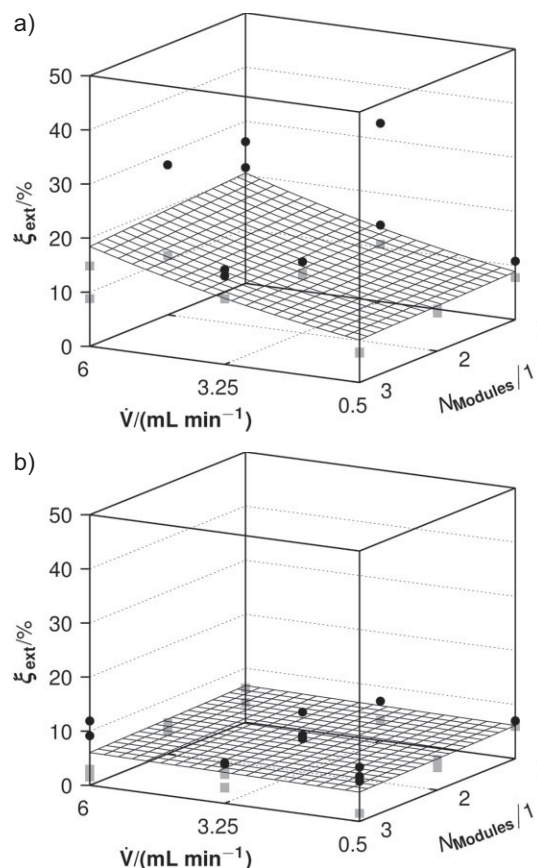


Figure 9. External photonic efficiency ξ_{ext} as a function of the number of modules and \dot{V} at $r_{\text{O}_2/\text{terp}} = 10.25$; (a) one OLED per module; (b) two OLEDs per module.

correlation between the ratio of the absorption and emission area is correct, the reactor setup with shifted reactors would increase the ratio by a factor of two and with this the efficiency of the reactor setup should be increased.

The performance of a setup with three modules and the CDW-030 light sources is illustrated in Fig. 12. The new-generation OLEDs can provide an improved conversion. A comparison with results where the first-generation OLEDs were used reveals that the influence of the increased irradiance depends strongly on the process conditions; see Tab. 3. This can mainly be explained by reaching the maximum conversion limit of 50 % or 100 %. Due to this restriction, a general degree of improvement cannot be demonstrated. Nevertheless, the results show a significant increase of conversion.

For easier comparison, the conversion improvement X_{imp} , defined as:

$$X_{\text{imp}} = \frac{X_{\text{Terp}}^{\text{CDW-030}}}{X_{\text{Terp}}^{\text{CDW-031}}} - 1 \quad (24)$$

was calculated. This number illustrates to which extent the higher photon flux enhances the conversion. Improvements in conversion larger than 100 % indicate that the magnitude of the emitted photon flux cannot directly be correlated to the

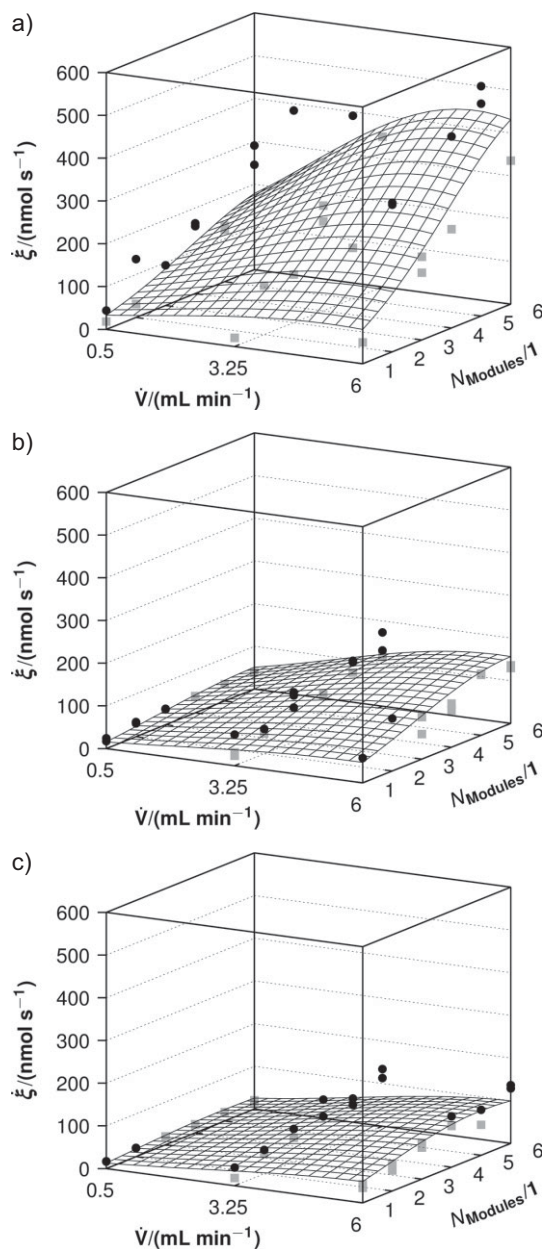


Figure 10. Productivity $\dot{\xi}$ as a function of the number of modules and \dot{V} at (a) $r_{O_2/RL} = 0.5$, (b) $r_{O_2/terp} = 10.25$ and (c) $r_{O_2/terp} = 20$ when utilizing one OLED per module.

expected improvement in conversion. It is assumed that the impact of reflection and/or scattering becomes more important as the emitted photon flux is increased.

As a result of the higher conversions, the productivity is also improved. The dependencies on the flow rate and the input ratio are similar to the results with first-generation OLEDs. The second-generation light sources improve the productivity by a factor of almost 4. Since the energy consumption stays nearly the same ($\eta_{lum} = 12.8\%$), this also corresponds to an increase of the overall energy efficiency by the same factor.

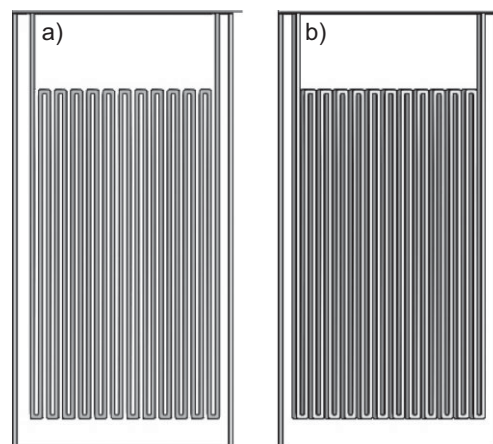


Figure 11. Comparison of the two reactor configurations. (a) Horizontally aligned reaction modules and (b) horizontally shifted reaction modules.

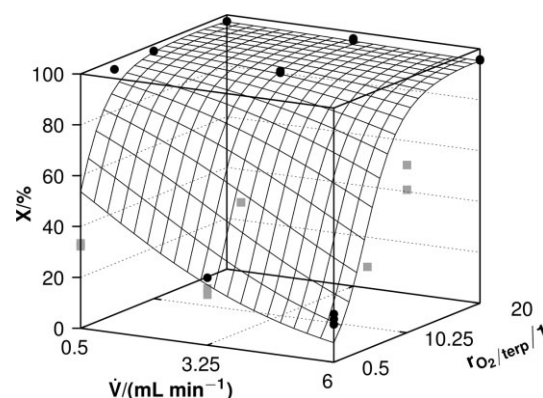


Figure 12. Conversion of α -terpinene as a function of \dot{V} and $r_{O_2/RL}$ of a setup with three modules utilizing two CDW-030 OLEDs each.

Table 3. Conversion X_{Terp} for different process conditions when the first-generation (CDW-031) or the second-generation (CDW-030) OLED panels were used.

\dot{V} [mL min ⁻¹]	$r_{O_2/terp}$	X_{Terp} [%]		X_{imp} [%]
		CDW-031	CDW-030	
0.5	0.5	19.1	32.2	168
0.5	10.25	89.3	97.4	109
0.5	20.0	92.5	97.5	105
3.25	0.5	15.4	22.3	145
3.25	10.25	44.4	96.2	217
3.25	20.0	41.5	97.4	235
6.0	0.5	3.3	14.9	453
6.0	10.25	20.4	65.9	324
6.0	20.0	33.9	95.5	282

Fig. 13 depicts the results for the new modules equipped with two reactors and two OLEDs each. Interestingly, no significant difference between the two investigated versions can be identified. This is attributed to reflection and scattering within the modules. The influence of these effects seems to be more important than the increased projection area. Further, it is worth noting that only slight differences in conversion can be observed when the reactor module with one reactor and the modules with two reactors are compared, i.e., compare Figs. 12 and 13. At a first glance, this seems to be unexpected since the residence time is doubled when modules with two reactors are used. The reason for this finding is that the number of OLEDs is kept constant. Thus, the emitted photon flux is the same in both module variants and the doubled residence time is counteracted by the doubled amount of α -terpinene, which is irradiated within the reactor modules. Hence, the amount of photons per amount of α -terpinene in a unit of time is constant, leading to similar results. These findings give evidence that the photon flux is the limiting factor even when second-generation OLEDs are utilized.

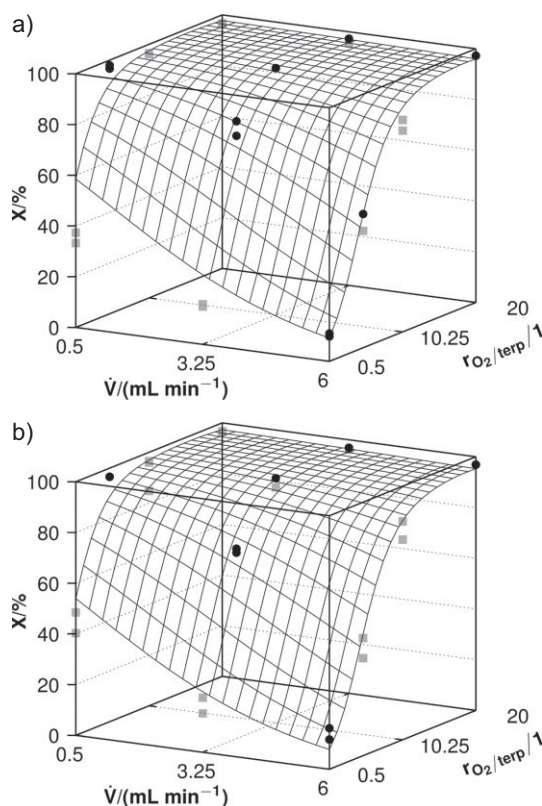


Figure 13. Conversion of α -terpinene as a function of \dot{V} and $r_{O_2/terp}$ of a setup; (a) with horizontally aligned reaction modules; (b) with horizontally shifted reaction modules.

4 Conclusions

A simple model for determining potential bottlenecks of a photoreactor setup is presented. While the model is not intended to fully describe all relevant processes, it reveals opti-

mization potentials and gives an insight into the sensitivity of the reactor setup to different optimization possibilities. With respect to the increasing research effort, such knowledge enables an even better utilization of the benefits of photochemical synthesis. A further advantage of the introduced balancing approach results from the concept of using only data already available from optimization studies of the process conditions. With this, additional effortful experiments are not essentially required.

Applying the developed concept to the characterization of a modular OLED reactor setup revealed huge optimization potential, especially with respect to the external photonic efficiency. Expressed in numbers, this translates to a total photonic efficiency below 20 %. This finding is especially important if such a system is considered for industrial application. Interestingly, the attempt to improve the external photonic efficiency by increasing the projection area of the reactor did not show any enhancement. This is attributed to a significant influence of reflection and scattering within the setup.

The results highlight the importance of an optimized design of microstructured photoreactors. Knowledge of photon fluxes within the different parts of the reactor setup is crucial to further exploit the potential of microstructured photoreactors since utilizing a well-characterized photoreactor enables the reduction of, e.g., experimental effort and/or operating costs.

The authors have declared no conflict of interest.

Symbols used

c	[mol L ⁻¹]	amount concentration
E	[varying]	irradiance
f	[-]	absorption factor
N	[-]	number of
\dot{n}	[mol s ⁻¹]	amount flux
q	[E s ⁻¹]	photon flux
r	[-]	stoichiometric ratio
s	[m]	optical length
S	[m ⁻²]	area
t	[s]	time
\dot{V}	[mL min ⁻¹]	flow rate
V	[mL]	volume
X	[-]	conversion

Greek letters

α	[m ⁻¹]	volumetric napierian absorption coefficient
Δ	[varying]	difference
η	[-]	efficiency
ξ	[mol s ⁻¹]	rate of conversion/productivity
ε	[m ² mol ⁻¹]	napierian molar absorption coefficient
λ	[nm]	wavelength
ϕ	[-]	quantum yield of ¹ O ₂ generation
ξ	[-]	photonic efficiency

Sub- and superscripts

abs	absorption
ext	external
<i>e</i>	radiometric quantity
g	gas
inc	incident
imp	improvement
l	liquid
lum	luminescent
<i>n</i>	amount basis
p	photonic quantity
R	reactor
refl	reflection
O ₂	oxygen
O ₂ /terp	oxygen to α -terpinene
S	area
terp	α -terpinene
Σ	total
λ	derivation to the wavelength (prefix spectral for quantities)
0	initial
1	at the end of the process

Abbreviation

OLED organic light-emitting diode

References

- [1] E. E. Coyle, M. Oelgemöller, *Photochem. Photobiol. Sci.* **2008**, 7, 1313–1322.
- [2] M. Oelgemöller, *Chem. Eng. Technol.* **2012**, 35, 1144–1152.
- [3] M. Oelgemöller, O. Shvydkiv, *Molecules* **2011**, 16, 7522–7550.
- [4] O. Shvydkiv, K. Nolan, M. Oelgemöller, *Beilstein J. Org. Chem.* **2011**, 7, 1055–1063.
- [5] K. Jähnisch, V. Hessel, H. Loewe, M. Baerns, *Angew. Chem. Int. Ed.* **2004**, 43, 406–446.
- [6] H. Ehrich, D. Linke, K. Morgenschweis, M. Baerns, K. Jähnisch, *CHIMIA Int. J. Chem.* **2002**, 56, 647–653.
- [7] K. Jähnisch, M. Baerns, V. Hessel, W. Ehrfeld, V. Haverkamp, H. Löwe, C. Wille, A. Guber, *J. Fluorine Chem.* **2000**, 105, 117–128.
- [8] K. F. Jensen, B. J. Reizman, S. G. Newman, *Lab Chip* **2014**, 14, 3206–3212.
- [9] O. Shvydkiv, S. Gallagher, K. Nolan, M. Oelgemöller, *Org. Lett.* **2010**, 12, 5170–5173.
- [10] K. Jähnisch, *Chem. Ing. Tech.* **2004**, 76, 630–632.
- [11] K. Jähnisch, U. Dingerdissen, *Chem. Eng. Technol.* **2005**, 28, 426–427.
- [12] B. D. A. Hook, W. Dohle, P. R. Hirst, M. Pickworth, M. B. Berry, K. I. Booker-Milburn, *J. Org. Chem.* **2005**, 70, 7558–7564.
- [13] S. Aida, K. Terao, Y. Nishiyama, K. Kakiuchi, M. Oelgemöller, *Tetrahedron Lett.* **2012**, 53, 5578–5581.
- [14] A. Yavorskyy, O. Shvydkiv, N. Hoffmann, K. Nolan, M. Oelgemöller, *Org. Lett.* **2012**, 14, 4342–4345.
- [15] A. Yavorskyy, O. Shvydkiv, K. Nolan, N. Hoffmann, M. Oelgemöller, *Tetrahedron Lett.* **2011**, 52, 278–280.
- [16] L. D. Elliott, J. P. Knowles, P. J. Koovits, K. G. Maskill, M. J. Ralph, G. Lejeune, L. J. Edwards, R. I. Robinson, I. R. Clemons, B. Cox et al., *Chem. Eur. J.* **2014**, 20, 15226–15232.
- [17] T. Aillet, K. Loubiere, O. Dechy-Cabaret, L. Prat, *Chem. Eng. Process.* **2013**, 64, 38–47.
- [18] T. Aillet, K. Loubiere, O. Dechy-Cabaret, L. Prat, *Int. J. Chem. Reactor Eng.* **2014**, 12, 257–269.
- [19] T. Aillet, K. Loubiere, L. Prat, O. Dechy-Cabaret, *AIChE J.* **2015**, 61, 1284–1299.
- [20] H. J. Kuhn, S. E. Braslavsky, R. Schmidt, *Pure Appl. Chem.* **2004**, 76, 2105–2146.
- [21] A. E. Cassano, C. A. Martin, R. J. Brandi, O. M. Alfano, *Ind. Eng. Chem. Res.* **1995**, 34, 2155–2201.
- [22] R. C. R. Wootton, R. Fortt, A. J. de Mello, *Org. Process. Res. Dev.* **2002**, 6, 187–189.
- [23] D. Ziegenbalg, G. Kreisel, D. Weiss, D. Kralisch, *Photochem. Photobiol. Sci.* **2014**, 13, 1005–1015.
- [24] K. N. Loponov, J. Lopes, M. Barlog, E. V. Astrova, A. V. Malkov, A. A. Lapkin, *Org. Process Res. Dev.* **2014**, 18, 1443–1454.
- [25] R. Battino, T. R. Rettich, T. Tominaga, *J. Phys. Chem. Ref. Data* **1984**, 13, 563–600.
- [26] F. Wilkinson, W. Helman, A. Ross, *J. Phys. Chem. Ref. Data* **1995**, 24, 663–1021.
- [27] F. Wilkinson, W. P. Helman, A. B. Ross, *J. Phys. Chem. Ref. Data* **1993**, 22, 113–262.
- [28] S. E. Braslavsky, A. M. Braun, A. E. Cassano, A. V. Emeline, M. I. Litter, L. Palmisano, V. N. Parmon, N. Serpone, *Pure Appl. Chem.* **2011**, 83, 931–1014.
- [29] S. Irandoust, B. Andersson, *Ind. Eng. Chem. Res.* **1989**, 28, 1684–1688.